

# Quantum geometry and local moment swapover in correlated graphene heterostructures

Niklas Witt  <sup>1,2,3,\*</sup> Siheon Ryee  <sup>2,\*</sup> Lennart Klebl  <sup>1,2</sup> Jennifer Cano  <sup>4,5</sup> Giorgio Sangiovanni  <sup>1</sup> and Tim O. Wehling  <sup>2,3</sup>

<sup>1</sup>*Institut für Theoretische Physik und Astrophysik and Würzburg-Dresden Cluster of Excellence ct.qmat, Universität Würzburg, 97074 Würzburg, Germany*

<sup>2</sup>*I. Institute of Theoretical Physics, Universität Hamburg, Notkestraße 9, 22607 Hamburg, Germany*

<sup>3</sup>*The Hamburg Centre for Ultrafast Imaging, Luruper Chaussee 149, 22761 Hamburg, Germany*

<sup>4</sup>*Department of Physics and Astronomy, Stony Brook University, Stony Brook, New York 11794, USA*

<sup>5</sup>*Center for Computational Quantum Physics, Flatiron Institute, New York, New York 10010, USA*

Graphene-based multilayer systems serve as versatile platforms for exploring the interplay between electron correlation and topology, thanks to distinctive low-energy bands marked by significant quantum metric and Berry curvature from graphene's Dirac bands. Here, we investigate Mott physics and local spin moments in Dirac bands hybridized with a flat band of localized orbitals in functionalized graphene. Via hybridization control, a topological transition is realized between two symmetry-distinct site-selective Mott states featuring local moments in different Wyckoff positions, with a geometrically enforced metallic state emerging in between. We find that this geometrically controlled local moment "swapover" and associated metal-insulator physics may be realized through proximity coupling of epitaxial graphene on SiC(0001) with group IV intercalants, where the Mott state faces geometrical obstruction in the large-hybridization limit. Our work shows that chemically functionalized graphene provides a correlated electron platform, very similar to the topological heavy fermions in graphene moiré systems but at significantly enhanced characteristic energy scales.

Graphene, initially celebrated as a weakly interacting Dirac material, has developed towards a material basis for correlated electron physics—in multilayer setups with lattice mismatch as well as twisted graphene multilayers, where the moiré potential localizes parts of the electronic states to form flat bands featuring strong electron correlations [1–19]. A seemingly complementary platform are moiré-less rhombohedral multilayers like Bernal bilayer, ABC trilayer, and ABCA quadrilayer where correlations emerge in absence of localized electronic orbitals but from itinerant electrons near Van Hove singularities [20–27]. As a common thread in both platforms, the low-energy states feature sizable Berry curvature and quantum metric, which are inherited from the graphene Dirac cones [28–31]. These quantum geometric contributions are suggested to play a decisive role in shaping emergent correlated states in these systems [32–36], including the stabilization of superconducting order [30, 37–48] and various kinds of (pseudo)magnetic states [49–55].

The emergent ordered states in moiré and rhombohedral multilayers set in at temperature scales of a few Kelvin or below, i.e.,  $\mathcal{O}(\text{meV})$  [2, 20]. What sets these scales is an open matter. Considering the most plausible moiré case from a strong-coupling perspective, the width of the flat bands ( $\sim 10 \text{ meV}$ ) and the hybridization gap ( $\sim 50 \text{ meV}$ ) determine order parameter stiffness, therefore also transition temperatures [39, 40, 47, 48]. These energy scales are essentially governed by the graphene interlayer tunellings and moiré potential modulations. It is questionable whether van der Waals engineering can significantly increase them beyond the current stage of graphene multilayer systems.

In this Letter, we propose an alternative material platform that exhibits strong quantum geometric effects and rich correlation phenomena, while also possessing a high intrinsic energy scale on the order of electronvolts. We first demonstrate

how hybridization of Dirac bands with localized orbitals and electron interactions lead to flat bands that feature "obstructed" Mottness: depending on the hybridization strength, the atomic limit of the emergent site-selective Mott states corresponds to local moments forming in distinct Wyckoff positions as identified by the Luttinger surface. Thus, a hybridization-induced topological transition between two symmetry-distinct site-selective Mott states takes place with a protected metallic state manifesting in between. We further show that the aforementioned topological transition can be partly realized in real materials through proximity coupling of epitaxial graphene on SiC(0001) with group IV intercalants.

*Hybridization control of flat bands: Quantum geometry and localization.* We start with an elemental model, inspired by early works on functionalized graphene [29, 56–68] as well as general considerations for flat band systems like Refs. [69–74]. We consider a bipartite lattice with sublattices A and B and one atom residing in each sublattice. We will refer to these atoms as A and B atoms, respectively. Sublattice A is furthermore assumed to be decorated with impurity atoms called X atoms. All atom species provide an orbital which transforms trivially under local point group operations. Due to the additional impurity, sublattice sites A and B belong to distinct Wyckoff positions of the crystallographic symmetry group. In Fig. 1a, we illustrate this setup for the example of a decorated two-dimensional honeycomb lattice, i.e., graphene with an impurity X. This geometry belongs to the wallpaper group  $p3m1$  (space group 156) with distinct high-symmetry Wyckoff positions 1a, 1b, and 1c on the sublattice sites and hexagon center, respectively, as shown in panel Fig. 1b.

The single-particle Hamiltonian generically reads  $H_0 = \sum_{\mathbf{k}\sigma} \Psi_{\mathbf{k}\sigma}^\dagger h(\mathbf{k}) \Psi_{\mathbf{k}\sigma}$  with  $\Psi_{\mathbf{k}\sigma} = (c_{A\mathbf{k}\sigma}, c_{B\mathbf{k}\sigma}, c_{X\mathbf{k}\sigma})^T$  where  $c_{m\mathbf{k}\sigma}$  is the annihilation operator for site  $m \in \{A, B, X\}$ , crystal mo-

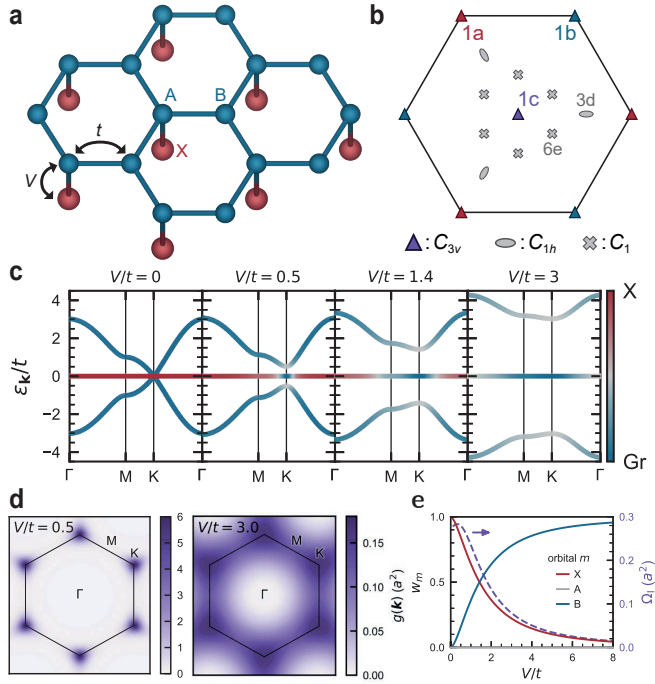


FIG. 1. Flat band hybridized to graphene. (a) Lattice structure of decorated graphene honeycomb lattice with impurity X hybridized to sublattice site A. Only hopping  $t$  between sublattices A and B as well as  $V$  between X and A exist. (b) Wyckoff positions and their respective local point symmetry groups for the wallpaper group  $p3m1$  (No. 156) representing the geometry in panel a. (c) Band structure for different values of  $V/t$ . The orbital character of the X and graphene atoms (A+B) are colored in red and blue, respectively. (d) Quantum metric  $g(\mathbf{k}) = g_{xx}(\mathbf{k}) + g_{yy}(\mathbf{k})$  of the band crossing the Fermi level at  $V/t = 0.5$  and  $V/t = 1.4$ . Note the different magnitude of scales. (e) Orbital weight  $w_m = \sum_{\mathbf{k}} |w_{km}|^2 / N_k$  ( $m \in \{A, B, X\}$ ) with weight  $|w_{km}|^2$  of the flat band crossing the Fermi level at  $\mathbf{k}$ , and minimal quadratic Wannier function spread  $\Omega_I$  as obtained from the quantum metric (c.f. Eq. (2)).

momentum  $\mathbf{k}$ , and spin  $\sigma$ .  $h(\mathbf{k})$  is given by

$$h(\mathbf{k}) = \begin{bmatrix} 0 & \xi(\mathbf{k}) & V \\ \xi^*(\mathbf{k}) & 0 & 0 \\ V^* & 0 & 0 \end{bmatrix}, \quad (1)$$

where  $\xi(\mathbf{k})$  is the Fourier transform of the hopping  $t$  between A and B atoms and  $V > 0$  the hopping between the X and the A atoms (c.f. Fig. 1a). For this Hamiltonian at half-filling, a zero-energy eigenstate  $|\mathbf{M}, \mathbf{k}\rangle = C_{\mathbf{k}}(0, V, -\xi(\mathbf{k}))^T$  with  $C_{\mathbf{k}} = 1/\sqrt{|\xi(\mathbf{k})|^2 + |V|^2}$  exists at any  $\mathbf{k}$ , independent of additional system specifics. Furthermore, for any finite  $V$  there is a finite gap separating the zero-energy band from the two other bands at  $\epsilon_{\pm}(\mathbf{k}) = \pm\sqrt{|\xi(\mathbf{k})|^2 + |V|^2}$ . This is shown for the decorated honeycomb lattice in Fig. 1c where the band structure with orbital/site-weight is shown for different values of  $V$ .

In the limiting case of dominating hybridization  $V \rightarrow \infty$ , we have  $|\mathbf{M}, \mathbf{k}\rangle \rightarrow (0, 1, 0)^T$ , which means that the flat band's state is entirely localized at the atoms of the non-decorated sublattice B. This is understandable from a strong bonding-

antibonding splitting between the  $|X\rangle$  and  $|A\rangle$  states that decouple from the system and push all the low-energy spectral weight into sublattice B. Wannierization of  $|\mathbf{M}, \mathbf{k}\rangle = (0, 1, 0)^T$  leads simply to a Wannier state in real space that is centered and completely peaked in sublattice B, thus the corresponding Wannier spread vanishes.

In the opposite limit of small hybridization  $t \gg V \rightarrow 0^+$ , the impurity atoms decouple and constitute the zero energy band  $|\mathbf{M}, \mathbf{k}\rangle \rightarrow (0, 0^+, -\xi(\mathbf{k})/|\xi(\mathbf{k})|)^T$  in the entire Brillouin zone except for the nodal point(s) where  $\xi(\mathbf{k}) = 0$  (c.f. Fig. 1c). The spectral weight of the flat band is correspondingly located at the impurity atoms in this limit. However, since there is no gap closure upon changing the hybridization while keeping it finite ( $V > 0$ ), the Wannier center *must not* have moved away from the B site. Conversely, while the Wannier center remains at B, the maxima of the Wannier centers shift to the three neighboring X sites, spreading over several atoms.

The variation in the Wannier spread is not an artifact but required by the quantum geometry of the zero-energy band: The gauge independent quadratic spread of Wannier functions,  $\Omega_I$ , is determined by the integral of the quantum metric [32, 37, 75–78]

$$\Omega_I = \frac{1}{N_k} \sum_{\mathbf{k}} g_{xx}(\mathbf{k}) + g_{yy}(\mathbf{k}) \leq \langle \mathbf{r}^2 \rangle - \langle \mathbf{r} \rangle^2 \quad (2)$$

which for single-bands measures the spread of maximally localized Wannier functions [77]. The quantum metric  $g(\mathbf{k})$  of the flat band is peaked at the nodes of  $\xi(\mathbf{k})$  for any finite  $V > 0$ . By increasing  $V$ , it starts to “leak out” by reducing in magnitude and being spread throughout the Brillouin zone, see Fig. 1d. Accordingly, the minimal spread  $\Omega_I$  takes a finite value for small  $V$  and goes to zero for  $V \rightarrow \infty$ . This is concomitant to the change in X-orbital weight of the flat band as is shown in Fig. 1e. Interestingly,  $\Omega_I$  is non-monotonous and displays a maximum for small  $V$  despite the quantum metric at the nodes monotonously increasing for  $V \rightarrow 0^+$  ( $g(\mathbf{k} = K) \sim 1/V^2$  for the honeycomb lattice in Fig. 1).

Localized orbitals hybridizing with a continuum of Dirac states, where the quantum metric of the resultant flat band is peaked in certain spots of the Brillouin zone, is not only realized in the functionalized graphene cases considered here ( $V \rightarrow 0^+$  limit). It similarly occurs in graphene moiré systems, as highlighted recently by the topological heavy fermion description of magic-angle twisted bilayer graphene [34].

*Symmetry-distinct site-selective Mott states.* We now investigate how Coulomb interactions conspire with the quantum geometry for the decorated honeycomb lattice. For simplicity, we assume a local Hubbard interaction  $U$  acting on all the atomic species. Our Hamiltonian  $\mathcal{H}$  thus has the following new term:

$$H_{\text{int}} = U \sum_m n_{m\uparrow} n_{m\downarrow}. \quad (3)$$

Here,  $\uparrow, \downarrow$  denote the electron spin and  $n_{m\uparrow(\downarrow)}$  the number operator. We set the effective local interaction  $U = 1.6t$  [79, 80],

which is well below the critical  $U$  for the Mott transition of the undecorated graphene [81]. For vanishing hybridization ( $V = 0$ ), graphene is a weakly correlated metal and the flat band of purely X character is a Mott insulator due to the lack of kinetic energy.

The interacting lattice model,  $\mathcal{H} = H_0 + H_{\text{int}}$ , is solved within dynamical mean-field theory (DMFT) [82]. The DMFT requires us to solve three independent impurity actions each for A, B, and X sites per self-consistency loop. We solve them using the numerically exact hybridization-expansion continuous-time quantum Monte Carlo method [83, 84]. The self-energy on the Matsubara axis is analytically continued to the real frequency axis using the maximum entropy method [85, 86].

We present the momentum-resolved spectral functions obtained from DMFT in Fig. 2a for three representative regimes of hybridization strength. It exhibits a clear presence of upper and lower Hubbard bands forming Mott gaps ( $\sim U$ ) in both the small and large  $V$  regimes [left and right panels] with a flat-band metallic phase intervening for intermediate value of  $V$  [middle panel]. Analyzing the underlying self-energy and the spin-spin correlation function reveals that X and B atoms are distinctly responsible for the aforementioned Mottness and concomitant formation of local spin moments in the respective regime. Under particle-hole symmetry, the simplest indicator to this behavior is the imaginary part of the local self-energy  $\text{Im}\Sigma(i\omega_0)$  at the lowest fermionic Matsubara frequency  $\omega_0 = \pi k_B T$  ( $T$  is temperature) because  $\text{Im}\Sigma$  diverges as  $\omega_n \rightarrow 0$  on the X (B) site for small (large)  $V$ . Its change with  $V$  is shown in Fig. 2b. We note that the emergence of the Dirac cone at the  $K$  point for small  $V$  in Fig. 2a is attributed to the vanishing weight of the X character on the flat band at the  $K$  point (c.f. Fig. 1b), which is otherwise gapped out everywhere else in the Brillouin zone due to the diverging  $\text{Im}\Sigma_X(i\omega_n \rightarrow 0)$ .

To better understand the above behavior, we closely examine the two extreme hybridization limits  $V \rightarrow 0^+$  and  $V \rightarrow \infty$ , where the spectral weight of the non-interacting flat band is predominantly made up of X and B sites, respectively. In these regimes, the local self-energy is well approximated by the Hubbard-I form [87]  $\Sigma_m(i\omega_n) = U^2/(4i\omega_n)$  ( $m = \text{X}$  at  $V \rightarrow 0^+$  and  $m = \text{B}$  at  $V \rightarrow \infty$ ). Consequently,  $\Sigma_m(i\omega_n) = 0$  for the other orbitals  $m \in \{\text{A}, \text{B}\}$  at  $V \rightarrow 0^+$  and  $m \in \{\text{A}, \text{X}\}$  at  $V \rightarrow \infty$ . The Hartree term of the self-energy is absorbed into the chemical potential.

Using the analytic form of the Hubbard-I self-energy, the nature of a topological phase transition is revealed by the Luttinger surface—the locus of  $\mathbf{k}$  where the zero-frequency Green's function  $G(\mathbf{k}, \omega = 0)$  exhibits zero eigenvalues or, equivalently, where the self-energy diverges at  $\omega = 0$  [88]. In our case, the Luttinger surface consists of a single band of Green's function zeros, which is purely of X character at  $V \rightarrow 0^+$  and B character at  $V \rightarrow \infty$ , respectively, because  $\text{Im}\Sigma_m(i\omega_n) = -U^2/(4\omega_n) \rightarrow -\infty$  for  $\omega_n \rightarrow 0^+$  in the respective limit. Since X and B sites reside on distinct Wyckoff positions 1a and 1b (c.f. Fig. 1b), the site-selective Mott states belong to two distinct irreducible representations or two dif-

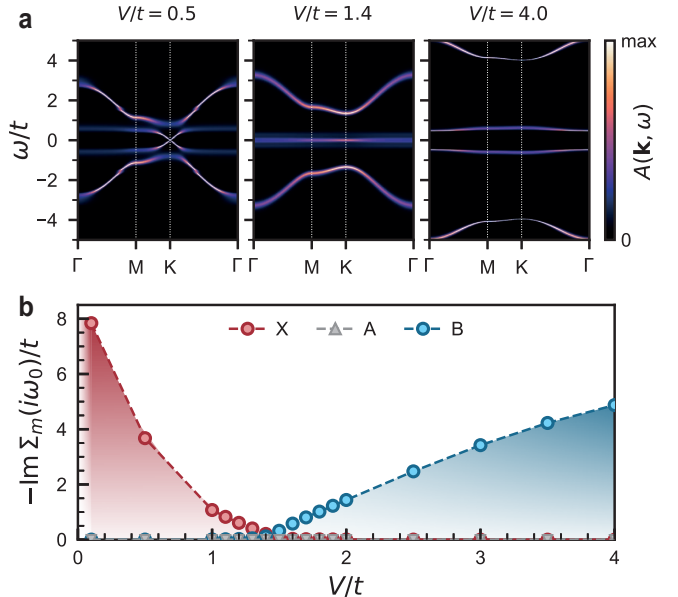


FIG. 2. Interacting decorated honeycomb model. (a) Momentum-resolved spectral functions from DMFT at  $T/t = 0.025$  and  $U/t = 1.6$ . From left to right for hybridization  $V/t = 0.5$ ,  $V/t = 1.4$ , and  $V/t = 4$ . (b) The imaginary part of the local self-energy at the lowest Matsubara frequency of X (red), A (gray), and B (blue) as function of  $V$ .

ferent atomic limits. Hence, the Luttinger surface cannot be deformed continuously by changing  $V$  without changing the number of zero bands or breaking symmetries. By preserving all the symmetries as in our DMFT calculations, an intermediate metallic phase as in the middle panel of Fig. 2a has to emerge where the Luttinger surface vanishes. This behavior as a function of  $V$  closely resembles the topological phase transition of noninteracting bands in the Su-Schrieffer-Heeger model [89, 90]. In our case, however, it is the topological phase transition of the “Mottness”, i.e., the positions of local spin moments, which is associated with the Green's function zeros (not poles) forming the Luttinger surface [91, 92].

*Proximity coupling of graphene and obstructed Mottness.* An obvious question concerns the realization of the topological transition between two distinct Mott insulating states in material setups. The decorated honeycomb lattice discussed in this work has been studied extensively in the context of  $sp$ -electron magnetism in graphene, which is a highly controversial topic in the literature [29, 56, 59, 60, 62–64, 67, 68]. Specifically, single-side covalently bonded impurities, like hydrogen or  $\text{CH}_3$  molecules [57–59, 61, 65, 66], on graphene correspond to the large  $V$  limit of our model.

A complimentary route of functionalization is given by proximity coupling of graphene sheets with suitable two-dimensional systems. Here, we focus on epitaxial graphene proximitized to group-IV adatoms at 1/3 monolayer coverage adsorbed on semiconducting surface. Without graphene, these surface lattice systems show various correlated phases [93–108]. Very recently, it was demonstrated that the addition

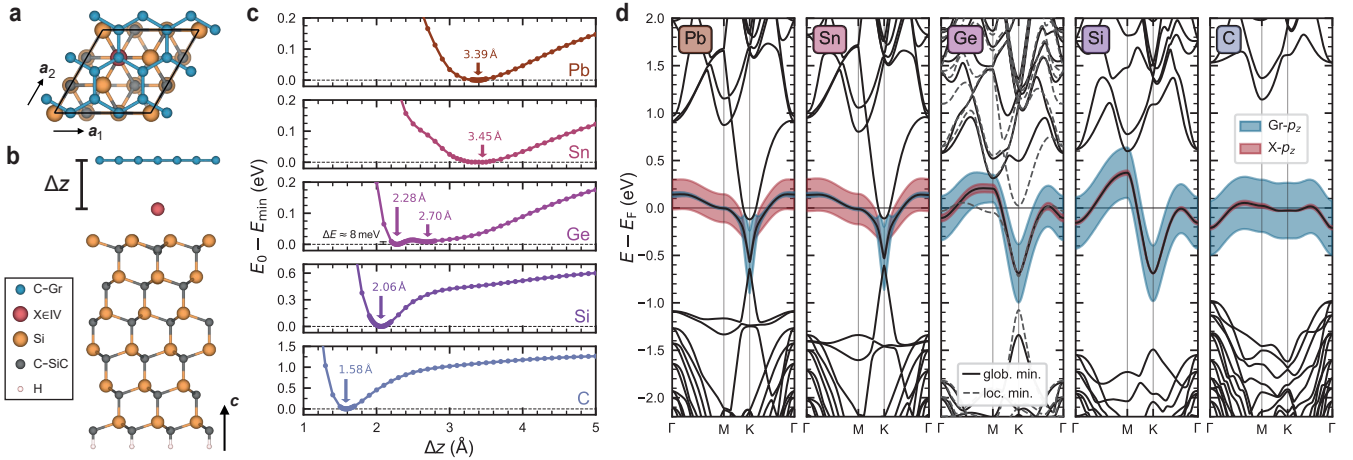


FIG. 3. Hybridization control via proximity coupling of epitaxial graphene and group-IV triangular adatom lattices. (a, b) Top and side view of the graphene/X/SiC(0001) heterostructure with distance  $\Delta z$  between the graphene layer and the X atom buffer layer of group IV elements. The X atoms are in a  $\sqrt{3} \times \sqrt{3}$  triangular lattice reconstruction on SiC(0001) and graphene stretched in a  $2 \times 2$  cell. (c) Energy as a function of layer distance  $\Delta z$  for different group IV atoms. The minimum energy  $E_{\min}$  is taken as zero and the minimum position is marked with an arrow. In case of X=Ge, two minima close in energy exist. (d) Band structure for the ground state structure for each IV element with the weight of the  $X-p_z$  and graphene- $p_z$  orbitals as fatband plots. For X=Ge, the band structure of the local minimum ( $\Delta z = 2.7 \text{ \AA}$ ) is drawn with dashed lines and no orbital weight.

of graphene to a Sn/SiC(0001) heterostructure host the site-selective Mott states which are strongly governed by hybridization effects [109].

In light of this observation, we investigate the electronic structure of graphene in proximity to different group-IV intercalants (X=C, Si, Ge, Sn, Pb) on a SiC(0001) substrate by using density functional theory (DFT) [110]. The general structure is shown in Figs. 3a and 3b. By tuning the intercalant species X, the distance  $\Delta z$  to the graphene layer is strongly changed in the ground state configuration, as the total energy curves in Fig. 3c demonstrate. Here, C intercalants are closest to the graphene layer with the equilibrium distance increasing by over 2 Å going down the periodic table. Notably, the ground state energy for Ge displays two local minima depending on  $\Delta z$ . The band structure for each X is drawn in Fig. 3d. They all display a relatively flat band pinned to the Fermi level from the intercalant's  $p_z$  orbitals hybridized to the Dirac bands of graphene. Due to the variation in equilibrium distances between graphene and the intercalant atoms the hybridization strength is widely tunable.

The band structures obtained from DFT can be rationalized with a generalization of our model to the  $2 \times 2$  unit cell structure with lower impurity density sketched in Fig. 4a. As in the  $1 \times 1$  case considered above (c.f. Figs. 1 and 2), we see from Fig. 4b that depending on the hybridization the spectral weight of the flat band moves from the X impurities ( $V \rightarrow 0^+$  limit) to sublattice B ( $V \gg t$  limit).

To assess the effect of electron correlations in this generalized model, we perform DMFT calculations using the same parameters as in the  $1 \times 1$  case. The resultant spectral functions are shown in Fig. 4c. We see that the limit of small  $V$  (like  $V/t = 0.5$ ) is very similar to the  $1 \times 1$  case above (c.f. Fig. 2a),

as there are well-formed Hubbard bands originating from the X orbitals and a correspondingly large  $|\text{Im}\Sigma_X(i\omega_0)| \gg t$  (c.f. Fig. 4b). Also similar to the  $1 \times 1$  case, increasing the hybridization quenches the Mott-Hubbard correlations at the X site, as can be seen from the decrease of  $|\text{Im}\Sigma_X(i\omega_0)|$  upon increasing  $V$  in Fig. 4b. Likewise, we find a metallic state with a flat band at the Fermi level for intermediate  $V/t = 1.5$ .

The  $V \rightarrow \infty$  case is interestingly different in the  $2 \times 2$  case as compared to the  $1 \times 1$  case. A pseudogap opens with weak but persisting spectral weight of the flat band at the Fermi level even at  $V \gg t$  (Fig. 4c, right panel), and we do not find a re-entrant divergent component of the self-energy for  $V \gg t$  (Fig. 4d). Instead, the self-energy takes a finite value at several atoms in sublattice B. This behavior can be understood as follows:

Since the density of X atoms is smaller in the  $2 \times 2$  graphene cell, undecorated A sublattice sites and percolating paths of non-decorated A and B atoms exist, see Fig. 4a. While this does not alter the physics of the small  $V$  limit where the spectral weight of the flat band primarily resides on the X atom, it changes the large  $V$  limit. Here, the spectral weight becomes distributed over all B sublattice sites and we obtain a robust and finite quantum metric at all  $V > 0$ , see panels b and e of Fig. 4. As a consequence, there is a geometric obstruction preventing the formation of a (site-selective) Mott state in the large  $V$  limit. This is captured by the local self-energy in Fig. 4d, which does not diverge on the B sites for  $V \rightarrow \infty$  in contrast to Fig. 2b. Hence, the momentum-resolved spectral function remains that of a correlated metal with the opening of a pseudogap when the majority of the (non-interacting) flat band's spectral weight lies on the B site, see Fig 4c. We added in Fig. 4d approximate hybridization values obtained

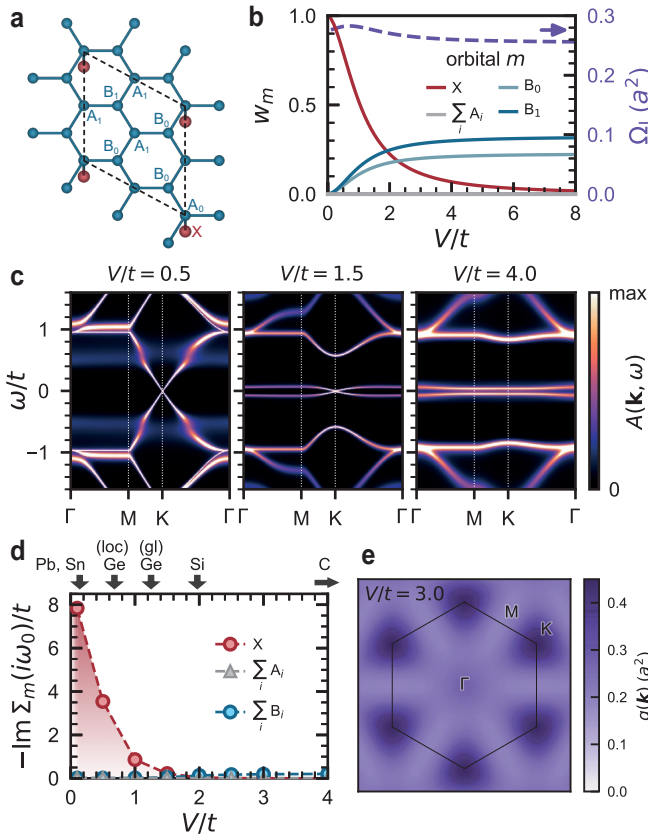


FIG. 4. Decorated graphene with smaller impurity density. (a) Unit cell of decorated graphene with 1/8 impurity X coverage as in Fig. 3a. The index of sublattice sites  $A_i$ ,  $B_i$  refer to distance from the impurity X. (b) Site-resolved weight  $w_m = \sum_k |w_{km}|^2/N_k$  ( $m \in \{A_i, B_i, X\}$ ) and minimal Wannier spread  $\Omega_l = \text{Tr } g_{ii}(k)$  of the flat band, similar to Fig. 1e. Note that  $\Omega_l$  does not vanish for  $V \rightarrow \infty$ . (c) Momentum-resolved spectral functions from DMFT at  $T/t = 0.025$  and  $U/t = 1.6$ . From left to right for hybridization  $V/t = 0.5$ ,  $V/t = 1.5$ , and  $V/t = 4$ . (d) The imaginary part of the local self-energy at the lowest Matsubara frequency of X (red), cumulative A sites (gray), and cumulative B sites (blue) as function of  $V$ . The hybridization values for different group IV atoms estimated from fitting the DFT bandstructures (Fig. 3d) are indicated with arrows. “loc” and “gl” refer to the local and global energy minimum’s configuration of Ge. (e) Quantum metric in the large hybridization limit.

from fitting tight-binding models to the DFT band structures from Fig. 3d, demonstrating that both hybridization limits are captured throughout all group IV atoms.

The correlated metallic state emerging here in the large  $V$  regime is stabilized by the quantum geometry of the flat band. The  $V \rightarrow \infty$  limit for this band is very similar to the vacancies and the vacancy induced flat band of Ref. [31].

*Conclusion.* In this work, we demonstrated a topological phase transition between symmetry-distinct site-selective Mott states and a geometrically stabilized metallic state enabled by hybridization control. We find that in between two states featuring local moments in different Wyckoff positions a correlated metallic state emerges for a most simple model of one-sublattice functionalized graphene. First principles cal-

culations demonstrate that similar physics of a site-selective Mott state transitioning to a geometrically stabilized flat-band metal can be likely realized in intercalated epitaxial graphene platforms. The series of group-IV intercalant atoms (C, Si, Ge, Sn, Pb) realize the entire range from weak ( $V \ll t$ ) to strong hybridization ( $V \gg t$ ).

The models discussed here are indeed very similar to the topological heavy fermion description of magic angle twisted bilayer graphene [34]. In both cases, there are localized orbitals hybridizing with Dirac bands resulting in a low-energy flat band with distinct quantum geometry. Distinctly, the flat bands in chemically functionalized graphene emerge at chemical energy scales, i.e., scales of covalent bonds and corresponding hoppings  $\sim t$ . Thus, the correlated flat band physics realized here can persist potentially up to higher temperatures than in twisted bilayer graphene. It appears very promising to explore other possible emergent ordered states, like magnetism and superconductivity, and the corresponding temperature scales in these covalently functionalized graphene systems.

*Acknowledgements.* We thank Lorenzo Crippa, Stefan Enzner, Titus Neupert, and Maia Vergniory for fruitful discussions. This work is supported by the Cluster of Excellence ‘CUI: Advanced Imaging of Matter’ of the Deutsche Forschungsgemeinschaft (DFG) - EXC 2056 - project ID 390715994, by DFG priority program SPP 2244 (WE 5342/5-1, project No. 422707584), the DFG research unit FOR 5242 (WE 5342/7-1, project No. 449119662), the DFG research unit FOR 5249 (“QUAST”, project No. 449872909). N.W. is additionally supported by the DFG funded SFB 1170 Tocotronics (project No. 258499086). J.C. acknowledges support from the Alfred P. Sloan Foundation through a Sloan Research Fellowship; from the Flatiron Institute, a division of Simons Foundation; and from the National Science Foundation under Grant No. DMR-1942447. Calculations were done on the supercomputer Lise at NHR@ZIB as part of the NHR infrastructure under the project hhp00056. The quantum metric was calculated using the divERGe library [111].

\* These two authors contributed equally.

- [1] L. Balents, C. R. Dean, D. K. Efetov, and A. F. Young, Superconductivity and strong correlations in moiré flat bands, *Nature Physics* **16**, 725 (2020).
- [2] K. P. Nuckolls and A. Yazdani, A microscopic perspective on moiré materials, *Nat. Rev. Mater.* **9**, 460 (2024), [arXiv:2404.08044](https://arxiv.org/abs/2404.08044).
- [3] Y. Cao, V. Fatemi, A. Demir, S. Fang, S. L. Tomarken, J. Y. Luo, J. D. Sanchez-Yamagishi, K. Watanabe, T. Taniguchi, E. Kaxiras, R. C. Ashoori, and P. Jarillo-Herrero, Correlated Insulator Behaviour at Half-Filling in Magic-Angle Graphene Superlattices, *Nature* **556**, 80 (2018).
- [4] Y. Cao, V. Fatemi, S. Fang, K. Watanabe, T. Taniguchi, E. Kaxiras, and P. Jarillo-Herrero, Unconventional Superconductivity in Magic-Angle Graphene Superlattices, *Nature* **556**, 43 (2018).

[5] X. Lu, P. Stepanov, W. Yang, M. Xie, M. A. Aamir, I. Das, C. Urgell, K. Watanabe, T. Taniguchi, G. Zhang, A. Bachtold, A. H. MacDonald, and D. K. Efetov, Superconductors, orbital magnets and correlated states in magic-angle bilayer graphene, *Nature* **574**, 653 (2019).

[6] M. Yankowitz, S. Chen, H. Polshyn, Y. Zhang, K. Watanabe, T. Taniguchi, D. Graf, A. F. Young, and C. R. Dean, Tuning superconductivity in twisted bilayer graphene, *Science* **363**, 1059 (2019).

[7] A. L. Sharpe, E. J. Fox, A. W. Barnard, J. Finney, K. Watanabe, T. Taniguchi, M. A. Kastner, and D. Goldhaber-Gordon, Emergent ferromagnetism near three-quarters filling in twisted bilayer graphene, *Science* **365**, 605 (2019).

[8] K. P. Nuckolls, M. Oh, D. Wong, B. Lian, K. Watanabe, T. Taniguchi, B. A. Bernevig, and A. Yazdani, Strongly correlated Chern insulators in magic-angle twisted bilayer graphene, *Nature* **588**, 610 (2020).

[9] M. Serlin, C. L. Tschirhart, H. Polshyn, Y. Zhang, J. Zhu, K. Watanabe, T. Taniguchi, L. Balents, and A. F. Young, Intrinsic quantized anomalous Hall effect in a moiré heterostructure, *Science* **367**, 900 (2020).

[10] C. Shen, Y. Chu, Q. Wu, N. Li, S. Wang, Y. Zhao, J. Tang, J. Liu, J. Tian, K. Watanabe, T. Taniguchi, R. Yang, Z. Y. Meng, D. Shi, O. V. Yazyev, and G. Zhang, Correlated states in twisted double bilayer graphene, *Nature Physics* **16**, 520 (2020).

[11] Z. Hao, A. M. Zimmerman, P. Ledwith, E. Khalaf, D. H. Najafabadi, K. Watanabe, T. Taniguchi, A. Vishwanath, and P. Kim, Electric field-tunable superconductivity in alternating-twist magic-angle trilayer graphene, *Science* **371**, 1133 (2021).

[12] S. Chen, M. He, Y.-H. Zhang, V. Hsieh, Z. Fei, K. Watanabe, T. Taniguchi, D. H. Cobden, X. Xu, C. R. Dean, and M. Yankowitz, Electrically tunable correlated and topological states in twisted monolayer–bilayer graphene, *Nature Physics* **17**, 374 (2021).

[13] J. M. Park, Y. Cao, K. Watanabe, T. Taniguchi, and P. Jarillo-Herrero, Tunable strongly coupled superconductivity in magic-angle twisted trilayer graphene, *Nature* **590**, 249 (2021).

[14] Y. Saito, J. Ge, L. Rademaker, K. Watanabe, T. Taniguchi, D. A. Abanin, and A. F. Young, Hofstadter subband ferromagnetism and symmetry-broken Chern insulators in twisted bilayer graphene, *Nature Physics* **17**, 478 (2021).

[15] S. Wu, Z. Zhang, K. Watanabe, T. Taniguchi, and E. Y. Andrei, Chern insulators, van Hove singularities and topological flat bands in magic-angle twisted bilayer graphene, *Nature Materials* **20**, 488 (2021).

[16] Y. Xie, A. T. Pierce, J. M. Park, D. E. Parker, E. Khalaf, P. Ledwith, Y. Cao, S. H. Lee, S. Chen, P. R. Forrester, K. Watanabe, T. Taniguchi, A. Vishwanath, P. Jarillo-Herrero, and A. Yacoby, Fractional Chern insulators in magic-angle twisted bilayer graphene, *Nature* **600**, 439 (2021).

[17] C. Rubio-Verdú, S. Turkel, Y. Song, L. Klebl, R. Samajdar, M. S. Scheurer, J. W. F. Venderbos, K. Watanabe, T. Taniguchi, H. Ochoa, L. Xian, D. M. Kennes, R. M. Fernandes, Á. Rubio, and A. N. Pasupathy, Moiré nematic phase in twisted double bilayer graphene, *Nature Physics* **18**, 196 (2022).

[18] J. M. Park, Y. Cao, L.-Q. Xia, S. Sun, K. Watanabe, T. Taniguchi, and P. Jarillo-Herrero, Robust superconductivity in magic-angle multilayer graphene family, *Nature Materials* **21**, 877 (2022).

[19] Y. Zhang, R. Polski, C. Lewandowski, A. Thomson, Y. Peng, Y. Choi, H. Kim, K. Watanabe, T. Taniguchi, J. Alicea, F. von Oppen, G. Refael, and S. Nadj-Perge, Promotion of superconductivity in magic-angle graphene multilayers, *Science* **377**, 1538 (2022).

[20] P. A. Pantaleón, A. Jimeno-Pozo, H. Sainz-Cruz, V. T. Phong, T. Cea, and F. Guinea, Superconductivity and correlated phases in non-twisted bilayer and trilayer graphene, *Nature Reviews Physics* **5**, 304 (2023).

[21] A. M. Seiler, F. R. Geisenhof, F. Winterer, K. Watanabe, T. Taniguchi, T. Xu, F. Zhang, and R. T. Weitz, Quantum cascade of correlated phases in trigonally warped bilayer graphene, *Nature* **608**, 298 (2022).

[22] Y.-C. Tsui, M. He, Y. Hu, E. Lake, T. Wang, K. Watanabe, T. Taniguchi, M. P. Zaletel, and A. Yazdani, Direct observation of a magnetic-field-induced Wigner crystal, *Nature* **628**, 287 (2024).

[23] Y. Zhang, R. Polski, A. Thomson, É. Lantagne-Hurtubise, C. Lewandowski, H. Zhou, K. Watanabe, T. Taniguchi, J. Alicea, and S. Nadj-Perge, Enhanced superconductivity in spin-orbit proximitized bilayer graphene, *Nature* **613**, 268 (2023).

[24] H. Zhou, T. Xie, A. Ghazaryan, T. Holder, J. R. Ehrets, E. M. Spanton, T. Taniguchi, K. Watanabe, E. Berg, M. Serbyn, and A. F. Young, Half- and quarter-metals in rhombohedral trilayer graphene, *Nature* **598**, 429 (2021).

[25] H. Zhou, T. Xie, T. Taniguchi, K. Watanabe, and A. F. Young, Superconductivity in rhombohedral trilayer graphene, *Nature* **598**, 434 (2021).

[26] H. Zhou, L. Holleis, Y. Saito, L. Cohen, W. Huynh, C. L. Patterson, F. Yang, T. Taniguchi, K. Watanabe, and A. F. Young, Isospin magnetism and spin-polarized superconductivity in Bernal bilayer graphene, *Science* **375**, 774 (2022).

[27] Z. Lu, T. Han, Y. Yao, A. P. Reddy, J. Yang, J. Seo, K. Watanabe, T. Taniguchi, L. Fu, and L. Ju, Fractional quantum anomalous Hall effect in multilayer graphene, *Nature* **626**, 759 (2024).

[28] T. O. Wehling, A. M. Black-Schaffer, and A. V. Balatsky, Dirac materials, *Advances in Physics* **63**, 1 (2014).

[29] M. I. Katsnelson, *The Physics of Graphene*, 2nd ed. (Cambridge University Press, 2020).

[30] L. Liang, T. I. Vanhala, S. Peotta, T. Siro, A. Harju, and P. Törmä, Band geometry, berry curvature, and superfluid weight, *Phys. Rev. B* **95**, 024515 (2017), arXiv:1610.01803.

[31] Q. Marsal and A. M. Black-Schaffer, Enhanced Quantum Metric due to Vacancies in Graphene, *Physical Review Letters* **133**, 026002 (2024).

[32] J. Yu, B. A. Bernevig, R. Queiroz, E. Rossi, P. Törmä, and B.-J. Yang, Quantum geometry in quantum materials (2024), arXiv:2501.00098 [cond-mat.mes-hall].

[33] H. C. Po, L. Zou, A. Vishwanath, and T. Senthil, Origin of Mott Insulating Behavior and Superconductivity in Twisted Bilayer Graphene, *Physical Review X* **8**, 031089 (2018).

[34] Z.-D. Song and B. A. Bernevig, Magic-Angle Twisted Bilayer Graphene as a Topological Heavy Fermion Problem, *Physical Review Letters* **129**, 047601 (2022).

[35] G. Rai, L. Crippa, D. Călugăru, H. Hu, F. Paoletti, L. de' Medici, A. Georges, B. A. Bernevig, R. Valentí, G. Sangiovanni, and T. Wehling, Dynamical Correlations and Order in Magic-Angle Twisted Bilayer Graphene, *Physical Review X* **14**, 031045 (2024).

[36] P. C. Adak, S. Sinha, A. Agarwal, and M. M. Deshmukh, Tunable moiré materials for probing berry physics and topology, *Nature Reviews Materials* **9**, 481 (2024).

[37] S. Peotta and P. Törmä, Superfluidity in topologically nontrivial flat bands, *Nat. Commun.* **6**, 8944 (2015), arXiv:1506.02815.

[38] P. Törmä, S. Peotta, and B. A. Bernevig, Superconductivity,

superfluidity and quantum geometry in twisted multilayer systems, *Nat. Rev. Phys.* **4**, 528 (2022).

[39] X. Hu, T. Hyart, D. I. Pikulin, and E. Rossi, Geometric and Conventional Contribution to the Superfluid Weight in Twisted Bilayer Graphene, *Physical Review Letters* **123**, 237002 (2019).

[40] F. Xie, Z. Song, B. Lian, and B. A. Bernevig, Topology-Bounded Superfluid Weight in Twisted Bilayer Graphene, *Phys. Rev. Lett.* **124**, 167002 (2020), 1906.02213.

[41] A. Julku, T. J. Peltonen, L. Liang, T. T. Heikkilä, and P. Törmä, Superfluid weight and Berezinskii-Kosterlitz-Thouless transition temperature of twisted bilayer graphene, *Physical Review B* **101**, 060505 (2020).

[42] J. Herzog-Arbeitman, V. Peri, F. Schindler, S. D. Huber, and B. A. Bernevig, Superfluid Weight Bounds from Symmetry and Quantum Geometry in Flat Bands, *Phys. Rev. Lett.* **128**, 087002 (2022), arXiv:2110.14663.

[43] K.-E. Huhtinen, J. Herzog-Arbeitman, A. Chew, B. A. Bernevig, and P. Törmä, Revisiting flat band superconductivity: Dependence on minimal quantum metric and band touchings, *Physical Review B* **106**, 014518 (2022).

[44] J. Yu, C. J. Ciccarino, R. Bianco, I. Errea, P. Narang, and B. A. Bernevig, Non-trivial quantum geometry and the strength of electron-phonon coupling, *Nature Physics* **20**, 1262 (2024).

[45] S. A. Chen and K. Law, Ginzburg-Landau Theory of Flat-Band Superconductors with Quantum Metric, *Physical Review Letters* **132**, 026002 (2024).

[46] J.-X. Hu, S. A. Chen, and K. T. Law, Anomalous coherence length in superconductors with quantum metric, *Communications Physics* **8**, 10.1038/s42005-024-01930-0 (2025).

[47] H. Tian, X. Gao, Y. Zhang, S. Che, T. Xu, P. Cheung, K. Watanabe, T. Taniguchi, M. Randeria, F. Zhang, C. N. Lau, and M. W. Bockrath, Evidence for Dirac flat band superconductivity enabled by quantum geometry, *Nature* **614**, 440 (2023).

[48] M. Tanaka, J. h.-j. Wang, T. H. Dinh, D. Rodan-Legrain, S. Zaman, M. Hays, A. Almanakly, B. Kannan, D. K. Kim, B. M. Niedzielski, K. Serniak, M. E. Schwartz, K. Watanabe, T. Taniguchi, T. P. Orlando, S. Gustavsson, J. A. Grover, P. Jarillo-Herrero, and W. D. Oliver, Superfluid stiffness of magic-angle twisted bilayer graphene, *Nature* **638**, 99 (2025).

[49] Z. Song, Z. Wang, W. Shi, G. Li, C. Fang, and B. A. Bernevig, All Magic Angles in Twisted Bilayer Graphene are Topological, *Physical Review Letters* **123**, 036401 (2019).

[50] J. Liu and X. Dai, Orbital magnetic states in moiré graphene systems, *Nature Reviews Physics* **3**, 367 (2021).

[51] Y. Shimazaki, M. Yamamoto, I. V. Borzenets, K. Watanabe, T. Taniguchi, and S. Tarucha, Generation and detection of pure valley current by electrically induced berry curvature in bilayer graphene, *Nature Physics* **11**, 1032 (2015).

[52] F. Wu and S. Das Sarma, Quantum geometry and stability of moiré flatband ferromagnetism, *Physical Review B* **102**, 165118 (2020).

[53] C. L. Tschirhart, M. Serlin, H. Polshyn, A. Shragai, Z. Xia, J. Zhu, Y. Zhang, K. Watanabe, T. Taniguchi, M. E. Huber, and A. F. Young, Imaging orbital ferromagnetism in a moiré Chern insulator, *Science* **372**, 1323 (2021).

[54] S. Grover, M. Bocarsly, A. Uri, P. Stepanov, G. Di Battista, I. Roy, J. Xiao, A. Y. Meltzer, Y. Myasoedov, K. Parreek, K. Watanabe, T. Taniguchi, B. Yan, A. Stern, E. Berg, D. K. Efetov, and E. Zeldov, Chern mosaic and berry-curvature magnetism in magic-angle graphene, *Nature Physics* **18**, 885 (2022).

[55] A. Abouelkomsan, K. Yang, and E. J. Bergholtz, Quantum met-  
ric induced phases in moiré materials, *Physical Review Research* **5**, 1012015 (2023).

[56] O. V. Yazyev and L. Helm, Defect-induced magnetism in graphene, *Physical Review B* **75**, 125408 (2007).

[57] D. W. Boukhvalov, M. I. Katsnelson, and A. I. Lichtenstein, Hydrogen on graphene: Electronic structure, total energy, structural distortions and magnetism from first-principles calculations, *Physical Review B* **77**, 035427 (2008).

[58] T. O. Wehling, M. I. Katsnelson, and A. I. Lichtenstein, Impurities on graphene: Midgap states and migration barriers, *Physical Review B* **80**, 085428 (2009).

[59] J. Zhou, Q. Wang, Q. Sun, X. S. Chen, Y. Kawazoe, and P. Jena, Ferromagnetism in Semihydrogenated Graphene Sheet, *Nano Letters* **9**, 3867 (2009).

[60] O. V. Yazyev, Emergence of magnetism in graphene materials and nanostructures, *Reports on Progress in Physics* **73**, 056501 (2010).

[61] T. O. Wehling, S. Yuan, A. I. Lichtenstein, A. K. Geim, and M. I. Katsnelson, Resonant Scattering by Realistic Impurities in Graphene, *Physical Review Letters* **105**, 056802 (2010).

[62] X. Hong, K. Zou, B. Wang, S.-H. Cheng, and J. Zhu, Evidence for Spin-Flip Scattering and Local Moments in Dilute Fluorinated Graphene, *Physical Review Letters* **108**, 226602 (2012).

[63] R. R. Nair, M. Sepioni, I.-L. Tsai, O. Lehtinen, J. Keinonen, A. V. Krasheninnikov, T. Thomson, A. K. Geim, and I. V. Grigorieva, Spin-half paramagnetism in graphene induced by point defects, *Nature Physics* **8**, 199 (2012).

[64] K. M. McCreary, A. G. Swartz, W. Han, J. Fabian, and R. K. Kawakami, Magnetic Moment Formation in Graphene Detected by Scattering of Pure Spin Currents, *Physical Review Letters* **109**, 186604 (2012).

[65] A. N. Rudenko, F. J. Keil, M. I. Katsnelson, and A. I. Lichtenstein, Exchange interactions and frustrated magnetism in single-side hydrogenated and fluorinated graphene, *Physical Review B* **88**, 081405 (2013).

[66] V. V. Mazurenko, A. N. Rudenko, S. A. Nikolaev, D. S. Medvedeva, A. I. Lichtenstein, and M. I. Katsnelson, Role of direct exchange and Dzyaloshinskii-Moriya interactions in magnetic properties of graphene derivatives: C2F and C2H, *Physical Review B* **94**, 214411 (2016).

[67] H. González-Herrero, J. M. Gómez-Rodríguez, P. Mallet, M. Moaied, J. J. Palacios, C. Salgado, M. M. Ugeda, J.-Y. Veuillet, F. Yndurain, and I. Brihuega, Atomic-scale control of graphene magnetism by using hydrogen atoms, *Science* **352**, 437 (2016).

[68] Z. Li, S. Li, Y. Xu, and N. Tang, Recent advances in magnetism of graphene from 0D to 2D, *Chemical Communications* **59**, 6286 (2023).

[69] D. Călugăru, A. Chew, L. Elcoro, Y. Xu, N. Regnault, Z.-D. Song, and B. A. Bernevig, General construction and topological classification of crystalline flat bands, *Nature Physics* **18**, 185 (2021).

[70] N. Regnault, Y. Xu, M.-R. Li, D.-S. Ma, M. Jovanovic, A. Yazdani, S. S. P. Parkin, C. Felser, L. M. Schoop, N. P. Ong, R. J. Cava, L. Elcoro, Z.-D. Song, and B. A. Bernevig, Catalogue of flat-band stoichiometric materials, *Nature* **603**, 824 (2022).

[71] P. M. Neves, J. P. Wakefield, S. Fang, H. Nguyen, L. Ye, and J. G. Checkelsky, Crystal net catalog of model flat band materials, *npj Computational Materials* **10**, 10.1038/s41524-024-01220-x (2024).

[72] J. Duan, C. Cui, M. Wang, W. Jiang, and Y. Yao, Three-Dimensional Multiorbital Flat Band Models and Materials, *Nano Letters* **24**, 15751 (2024).

[73] B. Bradlyn, L. Elcoro, J. Cano, M. G. Vergniory, Z. Wang,

C. Felser, M. I. Aroyo, and B. A. Bernevig, Topological quantum chemistry, *Nature* **547**, 298–305 (2017).

[74] J. Cano, B. Bradlyn, Z. Wang, L. Elcoro, M. G. Vergniory, C. Felser, M. I. Aroyo, and B. A. Bernevig, Building blocks of topological quantum chemistry: Elementary band representations, *Phys. Rev. B* **97**, 035139 (2018).

[75] N. Marzari and D. Vanderbilt, Maximally localized generalized Wannier functions for composite energy bands, *Physical Review B* **56**, 12847 (1997).

[76] R. Resta and S. Sorella, Electron Localization in the Insulating State, *Physical Review Letters* **82**, 370 (1999).

[77] N. Marzari, A. A. Mostofi, J. R. Yates, I. Souza, and D. Vanderbilt, Maximally localized Wannier functions: Theory and applications, *Reviews of Modern Physics* **84**, 1419 (2012).

[78] A. Marrazzo and R. Resta, Local Theory of the Insulating State, *Physical Review Letters* **122**, 166602 (2019).

[79] T. O. Wehling, E. Şaşioğlu, C. Friedrich, A. I. Lichtenstein, M. I. Katsnelson, and S. Blügel, Strength of Effective Coulomb Interactions in Graphene and Graphite, *Phys. Rev. Lett.* **106**, 236805 (2011).

[80] M. Schüller, M. Rösner, T. O. Wehling, A. I. Lichtenstein, and M. I. Katsnelson, Optimal hubbard models for materials with nonlocal coulomb interactions: Graphene, silicene, and benzene, *Phys. Rev. Lett.* **111**, 036601 (2013).

[81] M.-T. Tran and K. Kuroki, Finite-temperature semimetal-insulator transition on the honeycomb lattice, *Phys. Rev. B* **79**, 125125 (2009).

[82] A. Georges, G. Kotliar, W. Krauth, and M. J. Rozenberg, Dynamical mean-field theory of strongly correlated fermion systems and the limit of infinite dimensions, *Rev. Mod. Phys.* **68**, 13 (1996).

[83] E. Gull, A. J. Millis, A. I. Lichtenstein, A. N. Rubtsov, M. Troyer, and P. Werner, Continuous-time monte carlo methods for quantum impurity models, *Rev. Mod. Phys.* **83**, 349 (2011).

[84] C. Melnick, P. Sémond, K. Yu, N. D’Imperio, A.-M. Tremblay, and G. Kotliar, Accelerated impurity solver for DMFT and its diagrammatic extensions, *Computer Physics Communications* **267**, 108075 (2021).

[85] M. Jarrell and J. Gubernatis, Bayesian inference and the analytic continuation of imaginary-time quantum Monte Carlo data, *Physics Reports* **269**, 133 (1996).

[86] D. Bergeron and A.-M. S. Tremblay, Algorithms for optimized maximum entropy and diagnostic tools for analytic continuation, *Phys. Rev. E* **94**, 023303 (2016).

[87] J. Hubbard, Electron correlations in narrow energy bands, *Proceedings of the Royal Society of London. Series A. Mathematical and Physical Sciences* **276**, 238 (1963).

[88] I. Dzyaloshinskii, Some consequences of the luttinger theorem: The luttinger surfaces in non-fermi liquids and mott insulators, *Phys. Rev. B* **68**, 085113 (2003).

[89] W. P. Su, J. R. Schrieffer, and A. J. Heeger, Soliton excitations in polyacetylene, *Phys. Rev. B* **22**, 2099 (1980).

[90] J. K. Asbóth, L. Oroszlány, and A. Pályi, A short course on topological insulators, *Lecture notes in physics* **919** (2016).

[91] N. Wagner, L. Crippa, A. Amaricci, P. Hansmann, M. Klett, E. J. König, T. Schäfer, D. D. Sante, J. Cano, A. J. Millis, A. Georges, and G. Sangiovanni, Mott insulators with boundary zeros, *Nature Communications* **14**, 10.1038/s41467-023-42773-7 (2023).

[92] S. Bollmann, C. Setty, U. F. P. Seifert, and E. J. König, Topological Green’s Function Zeros in an Exactly Solved Model and Beyond, *Physical Review Letters* **133**, 136504 (2024).

[93] E. Ganz, F. Xiong, I.-S. Hwang, and J. Golovchenko, Submonolayer phases of pb on si(111), *Physical Review B* **43**, 7316 (1991).

[94] J. M. Carpinelli, H. H. Weitering, E. W. Plummer, and R. Stumpf, Direct observation of a surface charge density wave, *Nature* **381**, 398 (1996).

[95] J. M. Carpinelli, H. H. Weitering, M. Bartkowiak, R. Stumpf, and E. W. Plummer, Surface Charge Ordering Transition:  $\alpha$ -Phase of Sn/Ge(111), *Physical Review Letters* **79**, 2859 (1997).

[96] G. Profeta and E. Tosatti, Novel Electronically Driven Surface Phase Predicted in C/Si(111), *Physical Review Letters* **95**, 206801 (2005).

[97] G. Profeta and E. Tosatti, Triangular Mott-Hubbard Insulator Phases of Sn/Si(111) and Sn/Ge(111) Surfaces, *Physical Review Letters* **98**, 086401 (2007).

[98] S. Schuwalow, D. Grieger, and F. Lechermann, Realistic modeling of the electronic structure and the effect of correlations for Sn/Si(111) and Sn/Ge(111) surfaces, *Physical Review B* **82**, 035116 (2010).

[99] G. Li, M. Laubach, A. Fleszar, and W. Hanke, Geometrical frustration and the competing phases of the  $\text{Sn/Si}(111)\sqrt{3}\times\sqrt{3}R30^\circ$  surface systems, *Physical Review B* **83**, 041104 (2011).

[100] P. Hansmann, T. Ayral, L. Vaugier, P. Werner, and S. Biermann, Long-Range Coulomb Interactions in Surface Systems: A First-Principles Description within Self-Consistently Combined  $GW$  and Dynamical Mean-Field Theory, *Phys. Rev. Lett.* **110**, 166401 (2013).

[101] G. Li, P. Höpfner, J. Schäfer, C. Blumenstein, S. Meyer, A. Bostwick, E. Rotenberg, R. Claessen, and W. Hanke, Magnetic order in a frustrated two-dimensional atom lattice at a semiconductor surface, *Nature Communications* **4**, 10.1038/ncomms2617 (2013).

[102] S. Glass, G. Li, F. Adler, J. Aulbach, A. Fleszar, R. Thomale, W. Hanke, R. Claessen, and J. Schäfer, Triangular Spin-Orbit-Coupled Lattice with Strong Coulomb Correlations: Sn Atoms on a SiC(0001) Substrate, *Phys. Rev. Lett.* **114**, 247602 (2015).

[103] P. Hansmann, T. Ayral, A. Tejeda, and S. Biermann, Uncertainty principle for experimental measurements: Fast versus slow probes, *Scientific Reports* **6**, 10.1038/srep19728 (2016).

[104] M. Jäger, C. Brand, A. P. Weber, M. Fanciulli, J. H. Dil, H. Pfür, and C. Tegenkamp,  $\alpha$ -Sn phase on Si(111): Spin texture of a two-dimensional Mott state, *Phys. Rev. B* **98**, 165422 (2018).

[105] T. Nakamura, H. Kim, S. Ichinokura, A. Takayama, A. V. Zотов, A. A. Saranin, Y. Hasegawa, and S. Hasegawa, Unconventional superconductivity in the single-atom-layer alloy  $\text{Si}(111)\text{-}\sqrt{3}\times\sqrt{3}\text{-}(Tl,Pb)$ , *Phys. Rev. B* **98**, 134505 (2018).

[106] X. Cao, T. Ayral, Z. Zhong, O. Parcollet, D. Manske, and P. Hansmann, Chiral  $d$ -wave superconductivity in a triangular surface lattice mediated by long-range interaction, *Physical Review B* **97**, 155145 (2018).

[107] X. Wu, F. Ming, T. S. Smith, G. Liu, F. Ye, K. Wang, S. Johnston, and H. H. Weitering, Superconductivity in a Hole-Doped Mott-Insulating Triangular Adatom Layer on a Silicon Surface, *Physical Review Letters* **125**, 117001 (2020).

[108] F. Ming, X. Wu, C. Chen, K. D. Wang, P. Mai, T. A. Maier, J. Strockoz, J. W. F. Venderbos, C. González, J. Ortega, S. Johnston, and H. H. Weitering, Evidence for chiral superconductivity on a silicon surface, *Nature Physics* **19**, 500 (2023).

[109] C. Ghosal, S. Ryee, Z. Mamiyev, N. Witt, T. O. Wehling, and C. Tegenkamp, Electronic correlations in epitaxial graphene: Mott states proximitized to a relativistic electron

gas, [arxiv:2412.01329](https://arxiv.org/abs/2412.01329) (2024).

[110] The DFT calculations were carried out with the VASP code [112–114] using PBE functional [115] and PAW formalism [116, 117]. Plane-wave cutoff of 400 eV,  $k$ -mesh of  $12 \times 12 \times 1$  and DFT-D3 van der Waals corrections were used [118]. Relaxations of the structures until forces were smaller than 5 meV/Å were done. For each distance  $\Delta z$ , all atoms were allowed to move except the  $z$  positions of the X atom and the graphene C atom located directly above. This cell is an approximation of the full  $6\sqrt{3} \times 6\sqrt{3}$  that one finds in experiment, see Ref. [109]. The DFT data for the energetic minima – and in case of Ge also the additional local minimum – are deposited on the NOMAD repository [119] at doi:XXXXXXXXXX.

[111] J. B. Profe, D. M. Kennes, and L. Klelbl, divERGe implements various Exact Renormalization Group examples, *SciPost Physics Codebases* **10.21468/scipostphyscodeb.26** (2024).

[112] G. Kresse and J. Hafner, Ab initio molecular dynamics for liquid metals, *Phys. Rev. B* **47**, 558–561 (1993).

[113] G. Kresse and J. Furthmüller, Efficiency of ab-initio total energy calculations for metals and semiconductors using a plane-wave basis set, *Comput. Mater. Sci.* **6**, 15 (1996).

[114] G. Kresse and J. Furthmüller, Efficient iterative schemes for ab initio total-energy calculations using a plane-wave basis set, *Phys. Rev. B* **54**, 11169–11186 (1996).

[115] J. P. Perdew, K. Burke, and M. Ernzerhof, Generalized gradient approximation made simple, *Phys. Rev. Lett.* **77**, 3865–3868 (1996).

[116] P. E. Blöchl, Projector augmented-wave method, *Phys. Rev. B* **50**, 17953 (1994).

[117] G. Kresse and D. Joubert, From ultrasoft pseudopotentials to the projector augmented-wave method, *Phys. Rev. B* **59**, 1758 (1999).

[118] S. Grimme, J. Antony, S. Ehrlich, and H. Krieg, A consistent and accurate ab initio parametrization of density functional dispersion correction (DFT-D) for the 94 elements H-Pu, *The Journal of Chemical Physics* **132**, 154104 (2010).

[119] M. Scheidgen, L. Himanen, A. N. Ladines, D. Sikter, M. Nakhaei, A. Fekete, T. Chang, A. Golparvar, J. A. Márquez, S. Brockhauser, S. Brückner, L. M. Ghiringhelli, F. Dietrich, D. Lehmberg, T. Denell, A. Albino, H. Näsström, S. Shabih, F. Dobener, M. Kühbach, R. Mozumder, J. F. Rudzinski, N. Daelman, J. M. Pizarro, M. Kuban, C. Salazar, P. Ondračka, H.-J. Bungartz, and C. Draxl, NOMAD: A distributed web-based platform for managing materials science research data, *Journal of Open Source Software* **8**, 5388 (2023).